2024-07

Runx2 regulates peripheral nerve regeneration to promote Schwann cell migration and re-myelination

Hu, R

10.4103/1673-5374.387977
Neural Regeneration Research
Medknow

Runx2 regulates peripheral nerve regeneration to promote Schwann cell migration and re-myelination

Rong Hu[1,*], Xinpeng Dun[2], Lolita Singh[3], Matthew C. Banton[3]

https://doi.org/10.4103/1673-5374.387977

Date of submission: January 10, 2023

Date of decision: June 2, 2023

Date of acceptance: September 16, 2023

Date of web publication: November 8, 2023

Graphical Abstract

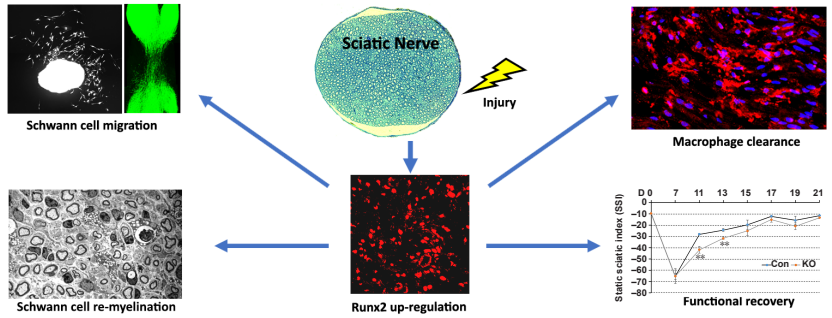

From the Contents

Abstract

Runx2 is a major regulator of osteoblast differentiation and function; however, the role of Runx2 in peripheral nerve repair is unclear. Here, we analyzed Runx2 expression following injury and found that it was specifically up-regulated in Schwann cells. Furthermore, using Schwann cell-specific Runx2 knockout mice, we studied peripheral nerve development and regeneration and found that multiple steps in the regeneration process following sciatic nerve injury were Runx2-dependent. Changes observed in Runx2 knockout mice include increased proliferation of Schwann cells, impaired Schwann cell migration and axonal regrowth, reduced re-myelination of axons, and a block in macrophage clearance in the late stage of regeneration. Taken together, our findings indicate that Runx2 is a key regulator of Schwann cell plasticity, and therefore peripheral nerve repair. Thus, our study shows that Runx2 plays a major role in Schwann cell migration, re-myelination, and peripheral nerve functional recovery following injury.

Key Words: macrophage clearance; migration; peripheral nerve injury; regeneration; re-myelination; Runx2; Schwann cells

Introduction

The peripheral nervous system has remarkable regenerative ability, and Schwann cell plasticity is key to successful repair following injury (Jessen and Mirsky, 2005, 2016; Min et al., 2020; Liu et al., 2023; Qin et al., 2023). Even in adult nerves, Schwann cells retain the ability to revert to a repair-competent phenotype following injury to create a permissive environment for regeneration (Jessen and Mirsky, 2016). In response to injury, adult Schwann cells in the distal nervous system produce growth factors, neurotrophins, cytokines, and extracellular matrix to promote neuronal survival and axon regeneration (Jessen and Mirsky, 2016; Ma et al., 2016; Cintron-Colon et al., 2022).

Studies have shown that the up-regulation of transcription factors such as c-Jun, Sox2, and cFos is essential for peripheral nerve repair (Arthur-Farraj et al., 2012; Fontana et al., 2012; Roberts et al., 2017; Ko et al., 2018; Dun et al., 2019). Recently published microarray and mRNA sequencing data have revealed a number of transcription factors whose expression is highly altered in Schwann cells following injury, but their function in nerve repair remains unclear (Barrette et al., 2010; Arthur-Farraj et al., 2012; Clements et al., 2017; Pan et al., 2017). One transcription factor that is dramatically up-regulated following peripheral nerve injury is Runt-related transcription factor-2 (Runx2), a member of the Runx-related transcription factor (Runxs) family (Hung et al., 2015; Arthur-Farraj et al., 2017). Runxs are evolutionarily conserved regulators of cell fate, and three family members (Runx1–3) have been identified in mammals (Schroeder et al., 2005; Bruderer et al., 2014; Otalora-Otalora et al., 2019). Runx1–3 contain runt DNA-binding domains and have well-established roles in hematopoietic (Runx1), bone (Runx2), and neuronal (Runx3) development (Cohen, 2009). Runx2$^{-/-}$ mice die perinatally because of failed osteoblast differentiation, indicating Runx2-dependent control of osteoblast-specific gene expression and its essential function in bone development and homeostasis (Komori et al., 1997; Otto et al., 1997).

Up-regulation of Runx2 in injured mouse sciatic nerve has been reported in several different transcriptome profiling studies (Barrette et al., 2010; Arthur-Farraj et al., 2012; Pan et al., 2017; Carr et al., 2019; Toma et al., 2020). However, the expression pattern of Runx2 in injured mouse sciatic nerve was not studied in detail. Furthermore, the function of Runx2 in peripheral nerve regeneration requires further elucidation. In this study, we aimed to investigate the cell types in the injured mouse sciatic nerve that express Runx2 and identify signals that regulate Runx2 expression following peripheral nerve injury. Importantly, we generated cell type-specific Runx2 knockout mice and induced sciatic nerve injury to understand the function of Runx2 in peripheral nerve regeneration.

Methods

Mouse breeding, peripheral nerve injury model, and functional recovery measurement

All animal experiments were approved by the Plymouth University Animal Welfare and Ethical Review Board (approval No. 30/3203) and designed and reported according to the Animal Research: Reporting of *In Vivo* Experiments (ARRIVE) guidelines (Percie du Sert et al., 2020). Mouse breeding and sciatic nerve surgery were carried out according to the regulations of Home Office under the UK Animals (Scientific Procedures) Act 1986. Runx2$^{fl/fl}$ mice were generated in Professor Karen Blyth's laboratory (School of Cancer Sciences, University of Glasgow) (Ferrari et al., 2015) on an FVB (Friend leukemia virus B) background. To generate Schwann cell-specific Runx2 knockout mice, we crossed Runx2$^{fl/fl}$ mice with P0-CRE (mP0-TOTA^{CRE}) mice (The Jackson Laboratory, Maine, USA, Strain: 017928, RRID: IMSR_JAX:017928; Feltri et al., 1999) to obtain Runx2$^{fl/fl}$ CRE-positive (knockout) and Runx$^{2fl/fl}$ CRE-negative (control) mice. To generate mice with green fluorescent protein (GFP)-labeled Schwann cells, Runx$^{2fl/fl}$ mice were crossed with PLP-GFP mice (Mallon et al., 2002; Dun et al., 2019) to obtain Runx2$^{fl/fl}$ Schwann cell-GFP-positive mice.

[1]School of Traditional Chinese Medicine, Department of Traditional Chinese Medicine, Nanfang Hospital, Southern Medical University, Guangzhou, Guangdong Province, China; [2]The Co-innovation Center of Neuroregeneration, Nantong University, Nantong, Jiangsu Province, China; [3]Faculty of Health, University of Plymouth, Plymouth, UK

*Correspondence to: Rong Hu, PhD, 522577026@qq.com.

https://orcid.org/0000-0001-9219-4524 (Rong Hu)

Funding: *This work was supported by the National Natural Science Foundation of China, No. 82104795 (to RH).*

How to cite this article: *Hu R, Dun X, Singh L, Banton MC (2024) Runx2 regulates peripheral nerve regeneration to promote Schwann cell migration and re-myelination. Neural Regen Res 19(7):1575-1583.*

Runx2$^{fl/fl}$:GFP-positive mice were then crossed with Runx2$^{fl/fl}$ CRE-positive mice to obtain Schwann cell-GFP-positive control and Runx2 knockout (KO) mice. Sciatic nerve crush or transection injury was performed as previously described (Dun and Parkinson, 2015). The mouse static sciatic index (SSI) was used to assess functional recovery (Baptista et al., 2007). Both male and female mice were used in this study. In total, 102 mice were used for all of the experiments. The control and Runx2 knockout mice were weighed on day 21 and day 30 after birth.

Recombinant proteins and primary and secondary antibodies

Recombinant mouse transforming growth factor β1 (Tgfβ1) (7666-MB), human Tenascin C (Tnc) (3358-TC), mouse betacellulin (Btc) (1025-CE), and human fibroblast growth factor 5 (Fgf5) (237-F5) (all purchased from R&D, Abingdon, UK), rabbit Runx2 antibody (1:1000, Cell Signaling Technology, Leiden, The Netherlands, Cat# 8486, RRID: AB_10949892), rabbit myelin protein zero (1:500 dilutions, Abcam, Cambridge, UK, Cat# ab31851, RRID: AB_2144668), rabbit myelin basic protein (1:500, Abcam, UK, Cat# ab40390, RRID: AB_1141521), chicken neurofilament heavy chain for immunohistochemistry (1:1000, Abcam, Cambridge, UK, Cat# ab4680, RRID: AB_304560), rabbit Iba1 (1:500, FUJIFILM Wako Chemicals Europe GmbH, Neuss, Germany, 019-19741, RRID: AB_839504), and mouse GAPDH (1:3000, EMD Millipore, Watford, UK, Cat# MAB374, RRID: AB_2107445) antibodies were used for immunolabeling and/or western blotting. Hoechst and donkey secondary antibodies conjugated with Alexa Fluor 488 (A21206, RRID: AB_2535792) or Alexa Fluor 568 (A10042, RRID: AB_2534017; A78950, RRID: AB_2921072), purchased from Thermo Fisher Scientific (Swindon, UK), were used for immunohistochemistry and diluted 1 to 500 for immunostaining. Horseradish peroxidase (HRP)-conjugated secondary antibodies (anti-rabbit, A1949, RRID: AB_257959, anti-mouse, A9309, RRID: AB_258443) used for western blotting were purchased from Sigma (Gillingham, UK) and diluted 1 to 3000.

Computational scRNA-seq data analysis and Affymetrix gene chip microarray data mining

The scRNA-seq data set GSE147285 for intact mouse sciatic nerve and post-injury day 3 distal nerve (sciatic nerve transection injury) (Toma et al., 2020) and data set GSE120678 for post-injury day 9 distal nerve (sciatic nerve transection injury) (Carr et al., 2019) were downloaded from the NCBI GEO database. Both data sets were analyzed using the Seurat v.3.2.1 (https://satijalab.org/seurat/) and sctransform v.0.3 R packages in R v.4.0.2 (https://cran.r-project.org/), as described in our recent publication (Chen et al., 2021). Runx2, Tgfβ1, Tnc, Btc, and Fgf5 gene expression data for intact and distal mouse sciatic nerve were obtained from the NCBI gene expression omnibus (GEO) (https://www.ncbi.nlm.nih.gov/geo/). Affymetrix gene chip microarray data sets GSE22291 (sciatic nerve crush injury) (Barrette et al., 2010), GSE74087 (sciatic nerve crush injury) (Pan et al., 2017) and GSE38693 (sciatic nerve transection injury) (Arthur-Farraj et al., 2012) were analyzed using the NCBI online tool GEO2R (https://www.ncbi.nlm.nih.gov/geo/geo2r/). The analyzed mRNA sequencing results for GSE103039 were downloaded from the supplemental files of the published paper by Clements et al. (2017).

mRNA purification, cDNA synthesis, reverse transcription-polymerase chain reaction, and quantitative reverse transcription-polymerase chain reaction

Total mRNA was extracted from sciatic nerves using an miRNeasy Mini Kit (Qiagen, Hilden, Germany, #217004). First-strand cDNA was synthesized with M-MLV reverse transcriptase (Promega, Southampton, UK, M368) using random hexamer primers (Promega, C1181). Reverse transcription-polymerase chain reaction (RT-PCR) was performed on a G-Storm GS4M instrument (Roche Applied Science, Basel, Switzerland). Quantitative RT-PCR (qRT-PCR) was performed on a PCR LightCycler480 Real-Time PCR Instrument (Roche Applied Science) using SYBR Green I master reaction mix (Roche Applied Science) with the following primers: Runx2 forward, 5′-ACC AAG TAG CCA GGT TCA AC-3′, Runx2 reverse, 5′-GAG GAT TTG TGA AGA CTG TTA TGG-3′, GAPDH forward, 5′-AAG GTC ATC CCA GAG CTG AA-3′, GAPDH reverse, 5′-CTG CTT CAC CAC CTT CTT GA-3′. The qRT-PCR conditions were as follows: denaturation at 95°C for 2 minutes, followed by 40 cycles of 95°C for 15 seconds, 60°C for 30 seconds, and 72°C for 30 seconds. Cross point (Cp) values were calculated using the LightCycler480 Real-Time PCR Instrument software. Relative mRNA levels were calculated using the 2(-Delta Delta C(T)) method (Livak and Schmittgen, 2001) and normalized to GAPDH as a reference gene. All reactions were carried out in triplicate for statistical analysis.

Schwann cell culture, tibial nerve explant experiments, and *in vivo* Schwann cell migration

Rat pups were obtained from the Plymouth Medical School Animal Facility and euthanized by cervical dislocation. Rat Schwann cells were prepared from the sciatic nerve and brachial plexus of 3-day-old Sprague-Dawley rat pups. Mouse Schwann cells were cultured from the distal sciatic nerve 7 days after transection injury (Woodley et al., 2019). Tibial nerves from GFP-positive control or Runx2 KO mice were cut into 2-mm pieces in a petri dish with a surgical blade. Nerve explants were transferred to 24-well plates and cultured in 1 mL low-glucose (1 g/mL) DMEM (D2902, Sigma) containing 10% FBS for 150 hours. GFP-positive migrating Schwann cells from tibial nerve explants were imaged using a LeicaIM8 fluorescence microscope (Leica, Wetzlar, Germany). Migrating Schwann cells were counted after the images were taken. *In vivo* Schwann cell migration was assessed at day 6 following sciatic nerve transection injury in both GFP-positive control and Runx2 KO mice. On day 6, transected sciatic nerves were harvested and fixed in 4% paraformaldehyde (in PBS, PH7.2, Sigma) at 4°C overnight. Nerves were cleared with 25%, 50%, and 75% glycerol (# 56-81-5, Sigma, in PBS) for imaging with a LeicaSPE confocal microscope (Leica). Z-stack images were taken and combined to measure the area of migrating Schwann cells (GFP-positive) in the nerve bridge.

Immunohistochemistry and immunocytochemistry

Sciatic nerves were dissected and fixed in 4% paraformaldehyde (in PBS, pH 7.2, Sigma) at 4°C overnight. Nerves were then washed in PBS (3 × 10 minutes) and dehydrated in 30% sucrose (in PBS, Sigma) overnight at 4°C. Subsequently, nerves were embedded in OCT medium (Agar Scientific, Stansted, UK) and sectioned on a cryostat (Leica) at a thickness of 12 µm. Schwann cells cultured on coverslips were fixed in 4% paraformaldehyde at 4°C for 15 minutes and then washed in PBS (3 × 10 minutes). Nerve sections or Schwann cells were then permeabilized with 0.25% Triton X-100 plus 1% bovine serum albumin (BSA) in PBS for 45 min and blocked with blocking buffer (3% BSA plus 0.05% Triton X-100 in PBS) for 1 hour at room temperature. Nerve sections or Schwann cells were incubated with primary antibodies (1:500 diluted in blocking buffer) overnight at 4°C. The next day, nerve sections or Schwann cells were washed with PBS (3 × 10 minutes) and then incubated with species-specific secondary antibodies plus Hoechst dye (1:1000 diluted in blocking buffer) for 1 hour at room temperature. Finally, nerve sections or Schwann cells were washed with PBS (3 × 10 minutes) and mounted with Citifluor (Agar Scientific, Stansted, UK, R1320) for imaging with a LeicaSPE confocal microscope (Leica). Images were taken from three repeats of neurofilament heavy chain-stained sections and four repeats of Iba1-stained nerve sections, and axon and macrophage numbers were counted in each section.

Western blotting and nerve tissue staining

Schwann cells were cultured in low-glucose (1g/mL) DMEM (Sigma) containing 3% FBS and treated with 10 ng/mL of Tgfβ1, Tnc, Btc, or FGF5 for 24 hours, or with 50 nM cAMP for 24, 48, or 72 hours. Following treatment, cells were lysed in 200 µL of radio-immunoprecipitation assay buffer plus phosphatase inhibitor cocktails (1:100, Santa Cruz Biotechnology, Dallas, TX, USA, sc-45045 and sc-45065). Cell lysates were centrifuged at 16,000 × *g* for 15 minutes at 4°C. The supernatants were transferred to new 1.5-mL tubes, and protein concentrations were determined using a Pierce™ BCA Protein Assay Kit (Thermo Fisher Scientific, Swindon, UK). A volume containing 20 µg of protein was then mixed with 4× sample buffer for electrophoresis. Nerves were harvested and directly sonicated in 1 × SDS loading buffer. Western blotting was performed as previously described (Woodley et al., 2019). ImageJ software (Version, 1.53r, National Institutes of Health, Bethesda, MD, USA; Schneider et al., 2012) was used to quantify the band intensity from three independent western blots.

5-ethynyl-2′-deoxyuridine labeling and cell proliferation assay

Cell proliferation was measured using the Click-iT™ EdU kit (Thermo Fisher Scientific, Swindon, UK). At 7 days post-injury, 2 mg of 5-ethynyl-2′-deoxyuridine (EdU; Invitrogen, Cheshire, UK, cat# C1033) was administered to each mouse via intraperitoneal injection (total volume 200 µL in DMSO/PBS), and 3 hours later the mice were sacrificed using CO_2. Sciatic nerves were collected and fixed in 4% paraformaldehyde overnight. The next day, the nerves were washed three times with PBS and then cryopreserved in 30% sucrose overnight. Subsequently, the nerves were embedded in OCT medium (Agar Scientific, Stansted, UK) and sectioned longitudinally on a cryostat (Leica) at a thickness of 10 µm. Sections were permeabilized with 0.25% Triton X-100 plus 1% BSA in PBS for 45 minutes and then blocked with blocking buffer (3% BSA plus 0.05% Triton X-100 in PBS) for 1 hour at room temperature. Next, sections of the sciatic nerve were incubated with the EdU Click-iT reaction cocktail (Invitrogen, Cheshire, UK, cat# C1033) for 30 min at room temperature, followed by 3 × 10 minutes PBS washes. The sections were incubated with rabbit anti-S100 primary antibodies (Agilent, Didcot, UK, #Z0311, RRID:AB, 10013383, 1:500 diluted in blocking buffer) overnight at 4ºC. The next day, the sections were washed with PBS (3 × 10 minutes) and then incubated with donkey and rabbit secondary antibodies (Thermo Fisher Scientific, Swindon, UK, A21206, RRID: AB_2535792) plus Hoechst dye (1:500 diluted in blocking buffer) for 1 hour at room temperature. Finally, the sections were washed with PBS and mounted with Citifluor (Agar Scientific, Stansted, UK, R1320) for imaging with a LeicaSPE confocal microscope (Leica). EdU and S100 double-positive cells were counted manually after the images were taken. Data were collected from four control and four Runx2 knockout mice.

Transmission electron microscopy

Sciatic nerves were fixed in 2.5% glutaraldehyde in 0.1 M cacodylate buffer (pH7.2) for 24 hours. The nerves were rinsed in cacodylate buffer and post-fixed in 1% osmium tetroxide in the same cacodylate buffer for 24 hours. Next, the nerves were rinsed in cacodylate buffer, dehydrated in an ascending ethanol series, and embedded in agar low-viscosity resin blocks. For transmission electron microscopy, ultra-thin sections were cut using a Leica EM UC7 ultramicrotome (Leica Microsystems GmbH, Wetzlar, Germany) and stained with uranyl acetate and lead citrate (Sigma). Sections were examined and photographed using a JEOL 1200EX or 1400 transmission electron microscope (TEM; JEOL UK Ltd., Welwyn Garden City, UK). The myelin thickness and axon perimeter of 200 myelinated fibers from three animals of each genotype were measured using ImageJ software (Version, 1.53r). The G-ratio was calculated as follows: axonal diameter/fiber (axon+myelin) diameter.

Mouse static sciatic index

The mouse static sciatic index (SSI) was measured to assess functional

recovery in control and Runx2 KO mice after sciatic nerve crush injury (Baptista et al., 2007). The SSI measurements were performed by an individual blinded to the genotype of the animals. Six animals of each genotype were assessed. Briefly, mice were placed in a clear acrylic display box (15 cm^3) and filmed with a digital camera from underneath. These videos were examined on computer, and selected frames were used for measurements of the print length and toe spread. The print length factor (PLF) and toe spread factor (TSF) were calculated as described previously (Baptista et al., 2007). SSI was calculated using the formula SSI = 101.3 × TSF – 54.03 × PLF – 9.5.

Statistical analysis

Sciatic nerve samples from three mice were pooled to generate enough material for one experimental repeat for qPCR and western blot; in total, nine animals were used to reach n = 3 in order to collect data for statistical analysis. Student's t-test was used to compare the control group with the treatment group. Results are presented as the mean ± SEM. Significance was defined as $P < 0.05$.

Results

Runx2 is up-regulated in mouse distal nerve Schwann cells following injury

Our research group is interested in understanding the function of transcription factors that are up-regulated in injured peripheral nerves (Doddrell et al., 2012, 2013; Mindos et al., 2017; Roberts et al., 2017; Dun et al., 2019). Recently, we analyzed cell type-specific gene up-regulation by single-cell RNA sequencing data analysis in intact and injured mouse sciatic nerves (Chen et al., 2021) and found that the transcription factor Runx2 was primarily up-regulated in Schwann cells associated with injured peripheral nerves (**Figure 1A** and **B**). Here, we analyzed Runx2 expression in the mouse distal nerve stump using three publicly available microarray data sets: GSE22291 (crush injury), GSE74087 (crush injury), and GSE38693 (transection injury) (Barrette et al., 2010; Arthur-Farraj et al., 2012; Pan et al., 2017). This analysis revealed that Runx2 is dramatically up-regulated in the mouse distal sciatic nerve stump following both sciatic nerve crush injury and transection injury (**Figure 1C** and **D**). At day 7 post-injury, Runx2 showed a significantly higher fold change ($P < 0.001$) in up-regulation in the distal sciatic nerve than either c-Jun or Sox2, two well characterized and regulated transcription factors (Parkinson et al., 2008; Parrinello et al., 2010; Arthur-Farraj et al., 2012; Fontana et al., 2012; Roberts et al., 2017; Dun et al., 2019) (**Figure 1C**). Following the microarray data analysis, we performed qRT-PCR analysis in a mouse (C57/BL6) model of sciatic nerve transection injury and observed dramatic up-regulation of Runx2 mRNA expression up to 14 days post-injury (**Figure 1E**). We next examined Runx2 protein expression in cultured rat primary Schwann cells and in sciatic nerve sections 7 days after injury in PLP-GFP mice (in which Schwann cells are labeled with GFP) (Mallon et al., 2002; Chen et al., 2019). Immunostaining demonstrated strong Runx2 expression in cultured rat Schwann cells (**Figure 1F**), and the *in vivo* staining results confirmed that Runx2 was primarily up-regulated in Schwann cells (GFP-positive) associated with the distal nerve following injury (**Figure 1G–N**).

Autocrine signals promote Runx2 expression in Schwann cells

Runx2 is best known for inducing osteoblast differentiation, which also involves up-regulation of Tgfβ1 expression (Lee et al., 2000). Previous studies have shown that Tgfβ1 is up-regulated in the distal sciatic nerve following injury (Scherer et al., 1993; Rufer et al., 1994; Kiefer et al., 1995; Parkinson et al., 2001; Clements et al., 2017; Toma et al., 2020). We therefore analyzed the expression levels of Tgfβ1 and three other highly up-regulated extracellular signaling molecules, Tenascin-C (Tnc) (Zhang et al., 2016), Betacellulin (Btc) (Vallieres et al., 2017) and Fgf5 (Chen et al., 2020), to identify factors that regulate Runx2 expression in cultured primary rat Schwann cells. These selected proteins were not only highly up-regulated in the distal nerve stump (**Figure 2A–D**), but also play important roles in promoting peripheral nerve regeneration. Our findings showed that Tnc, Btc, and Fgf5 all significantly up-regulated Runx2 expression in Schwann cells; however, to our surprise, Tgfβ1 significantly decreased Runx2 protein expression ($P < 0.001$; **Figure 2G** and **H**). Analyzing the published mRNA sequencing data set GSE103039, which assessed cultured rat primary Schwann cells following Tgfβ1 treatment (Clements et al., 2017), showed that Tgfβ1 significantly inhibited Runx2 mRNA expression in cultured rat primary Schwann cells (**Figure 2E** and **F**).

Owing to the opposing effects of Tgfβ1 *versus* Btc, Tnc, and Fgf5 on Runx2 expression in Schwann cells, we compared their cell type-specific expression in the distal nerve stump at day 3 and day 9 post-injury using the scRNA-seq data sets mentioned above. This analysis showed that, similar to the pattern of Runx2 up-regulation observed in Schwann cells, Btc, Fgf5, and Tnc were primarily expressed in Schwann cells (**Figure 2L–Q**). In contrast, Tgfβ1 was undetectable in any cell type at day 3 post-injury, whereas at day 9 post-injury it was highly expressed in endothelial cells associated with the injured peripheral nerves (**Figure 2R**). Thus, it appears that Schwann cell-derived autocrine signals promote Runx2 expression in Schwann cells following injury, while Tgfβ1 produced by endothelial cells inhibits Runx2 expression in Schwann cells.

Btc and Fgf signaling have both been shown to promote Schwann cell re-myelination during peripheral nerve regeneration (Allodi et al., 2014; Vallieres et al., 2017). Therefore, we next treated cultured rat Schwann cells with cyclic AMP (cAMP) to induce a myelinating phenotype and assessed Runx2 expression by western blot. cAMP treatment up-regulated the expression of myelin protein zero (Mpz) in cultured rat Schwann cells after 48 hours (**Figure 2I**). Interestingly, cAMP treatment also increased Runx2 expression in cultured

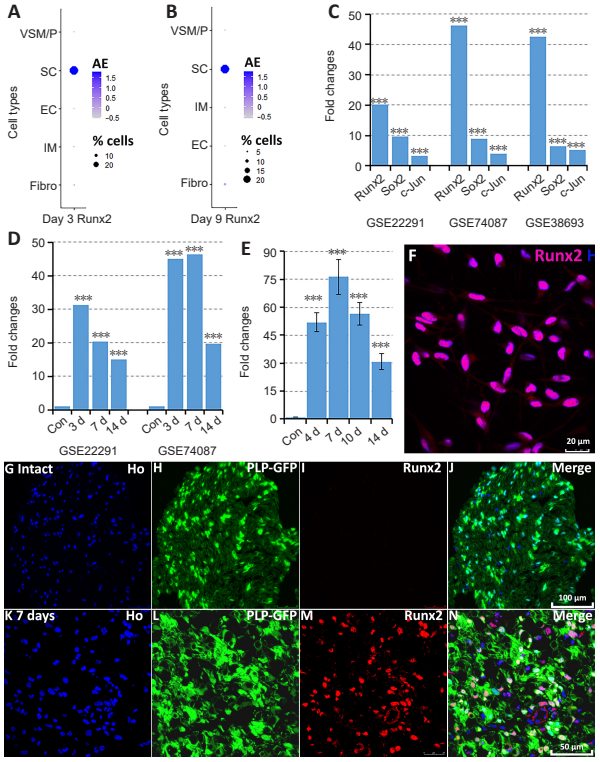

Figure 1 | **Runx2 up-regulation in Schwann cells following peripheral nerve injury.**
(A) Single-cell transcriptome data (GSE147285, sciatic nerve transection injury) analysis showing that Runx2 was up-regulated in Schwann cells associated with the distal nerve stump on day 3 post-injury. (B) Single-cell transcriptome data (GSE120678, sciatic nerve transection injury) analysis showing that Runx2 was up-regulated in Schwann cells associated with the distal nerve stump on day 9 post-injury. EC: Endothelial cells; Fibro: fibroblasts; IM: immune cells; SC: Schwann cells; VSM/P: vascular smooth muscle cells and pericytes. (C) Fold changes in Runx2, Sox2, and c-Jun expression in the mouse distal sciatic nerve on day 7 post-injury; data from GSE22291 (crush injury), GSE74087 (crush injury), and GSE38693 (transection injury). (D) Runx2 up-regulation in the distal nerve stump on days 3, 7, and 14 following sciatic nerve crush injury; data from GSE22291 and GSE74087. (E) Quantitative reverse transcription-polymerase chain reaction (qRT-PCR) validation of Runx2 mRNA up-regulation in the distal sciatic nerve on days 4, 7, 10, and 14 following sciatic nerve transection injury, n = 3. ***$P < 0.001$ in C and D; fold changes and P-values were calculated using the NCBI online software program GEO2R by comparing the injury group to the control group. The quantitative reverse transcription-polymerase chain reaction data in E were analyzed using Student's t-test) by comparing the injury group to the control group. Data are presented as the mean ± SEM. (F) Immunostaining for Runx2 (red) in cultured primary rat Schwann cells. (G–J) Immunostaining for Runx2 in intact sciatic nerve transverse cryosections from PLP-GFP (green fluorescent protein) mice showing that Runx2 is not expressed in the intact sciatic nerve; GFP (green) indicates Schwann cells. (K–N) Immunostaining for Runx2 in day 7 distal sciatic nerve transverse cryosections from PLP-GFP mice showing that Runx2 is up-regulated in GFP-positive Schwann cells. Blue in G and K indicates cell nuclei, green in H and L indicates GFP-positive Schwann cells, and red in I and M indicates Runx2. Scale bars: 20 μm in F, 100 μm in J, and 50 μm in N.

rat Schwann cells (**Figure 2I** and **J**). In line with our findings, Ding et al. previously reported that cAMP treatment up-regulated Runx2 expression in cultured Schwann cells (Ding et al., 2018). These findings indicate that Runx2 up-regulation in Schwann cells following adult peripheral nerve injury may promote Schwann cell re-differentiation during peripheral nerve regeneration. In subsequent experiments, we sought to test this putative function *in vivo*.

Normal development of Schwann cell-specific Runx2 knockout nerves

To better understand the role of Runx2 in Schwann cells during peripheral nerve regeneration, we crossed $Runx2^{fl/fl}$ mice (Ferrari et al., 2015) with P0-CRE (mP_0-TOTACRE) mice (Feltri et al., 1999) to generate Schwann cell-specific Runx2 KO mice. Complete Runx2 knockout in Schwann cells was confirmed by western blot (**Figure 3A**) and immunostaining (**Figure 3G–N**) on day 7 post-sciatic nerve transection. A previous study reported that Runx2 global null mice died soon after birth due to ossification failure (Otto et al., 1997). However, our Schwann cell-specific Runx2 KO mice were viable and exhibited normal body weights compared with control mice ($Runx2^{fl/fl}$ CRE negative) of the same age (**Figure 3D** and **E**). Furthermore, western blotting revealed similar levels of Mpz and myelin basic protein (Mbp) in control and Runx2 KO mice (**Figure 3B** and **C**). Next, we assessed Runx2 mRNA expression in the developing sciatic nerve of wild-type mice and found that all Runx2 mRNA counts were below 2 reads per kilobase of transcript per million reads mapped (RPKM) from embryonic day 13 to postnatal day 60 (**Figure 3F**). Following sciatic nerve injury on day 5, the Runx2 mRNA count increased to 64.36 RPKM (**Figure 3F**), suggesting that Runx2 is expressed at very low levels in the developing mouse sciatic nerve. In agreement with this, examination of

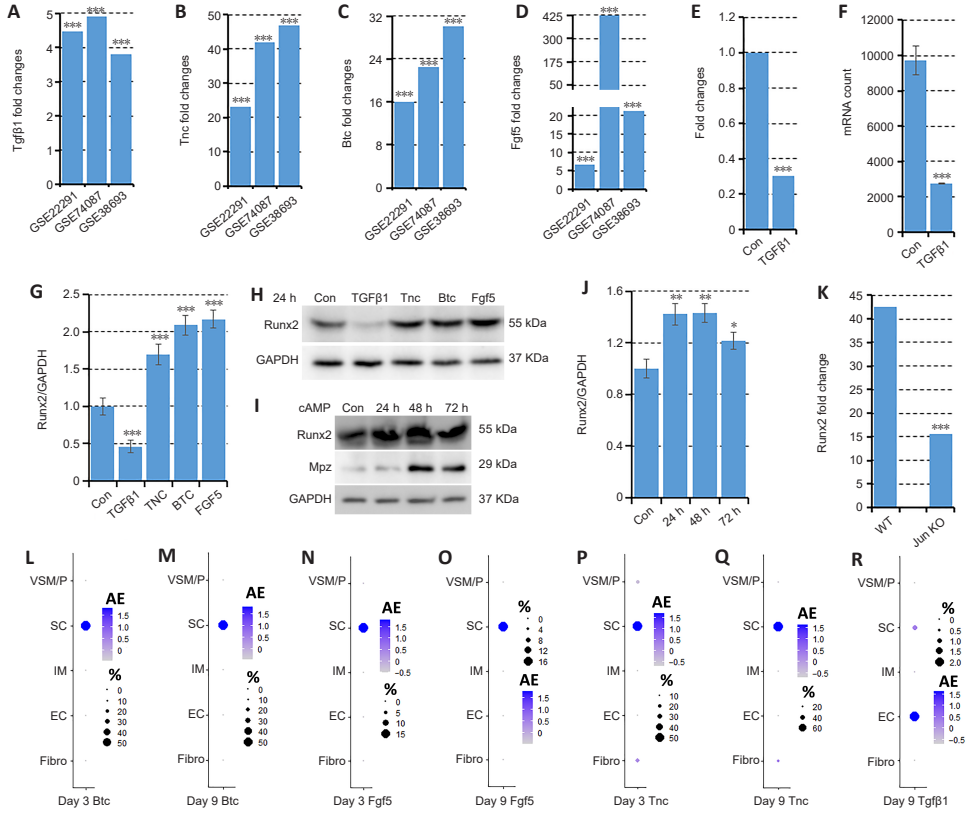

Figure 2 | **Tnc, Btc, and Fgf5 up-regulate Runx2 expression in Schwann cells.**
(A–D) Tgfβ1, Tnc, Btc, and Fgf5 expression in mouse distal nerves on day 7 following sciatic nerve injury; data from GSE22291 (crush injury), GSE74087 (crush injury), and GSE38693 (transection injury). (E) Fold changes in Runx2 mRNA expression in cultured rat Schwann cells upon Tgfβ1 treatment; data from GSE103039. (F) Runx2 mRNA counts in cultured rat Schwann cells upon Tgfβ1 treatment; data from GSE103039. (G) Quantification of Runx2 protein expression after 24 hours of Tgfβ1, Tnc, Btc, or Fgf5 treatment; results from three independent western blots. (H) Western blot showing that Tnc, Btc, and Fgf5 up-regulate Runx2 in rat Schwann cells after 24 hours of treatment, while Tgfβ1 inhibits Runx2 expression. (I) Western blot showing Runx2 protein up-regulation in cultured rat Schwann cells after 24, 48, and 72 hours of cAMP treatment. (J) Quantification of Runx2 expression induced by cAMP treatment, as assessed by three independent western blots. GAPDH: Glyceraldehyde-3-phosphate dehydrogenase. (K) Fold changes in Runx2 expression in the distal sciatic nerves of control and Schwann cell-specific c-Jun knockout mice on day 7 post-injury; data from GSE38693. (L) Single-cell transcriptome data analysis showing Btc expression in Schwann cells associated with the distal nerve stump on day 3 post-injury. (M) Single-cell transcriptome data analysis showing Btc expression in Schwann cells associated with the distal nerve stump on day 9 post-injury. (N, O) Single-cell transcriptome data analysis showing Fgf5 expression in Schwann cells associated with the distal nerve stump on day 3 (N) and day 9 post-injury (O). (P, Q) Single-cell transcriptome data analysis showing Tnc expression in Schwann cells associated with the distal nerve stump on day 3 (P) and day 9 post-injury (Q). (R) Single-cell transcriptome data analysis showing Tgfβ1 expression in endothelial cells associated with the distal nerve stump on day 9 post-injury. Fibro: fibroblasts; IM: immune cells; SC: Schwann cells; EC: endothelial cells; VSM/P: vascular smooth muscle cells and pericytes. Data are presented as the mean ± SEM. *$P < 0.05$, **$P < 0.01$, ***$P < 0.001$. In A–D, fold changes and P-values were obtained using the NCBI online software program GEO2R by comparing the injury group to the control group. In E and F, the data were analyzed using Student's t-test by comparing Tgfβ1 treatment to the control group. In K, the data were analyzed using Student's t-test by comparing wild type mice with c-Jun knockout mice.

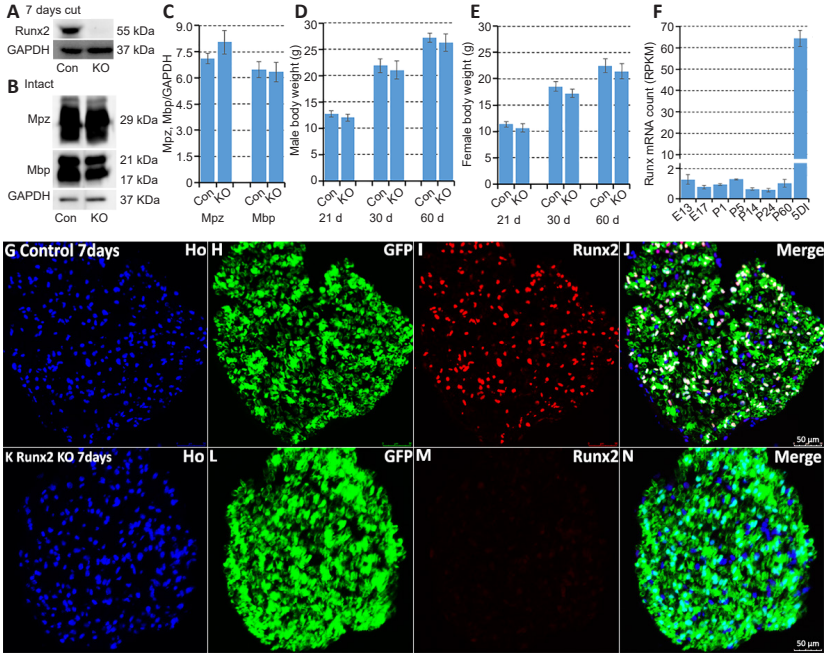

Figure 3 | **Generating Schwann cell-specific Runx2 knockout mice.**
(A) Runx2 protein is undetectable in Runx2 KO mice by western blot of distal sciatic nerve tissue on day 7 following sciatic nerve transection. (B) Western blot comparing the levels of Mpz and Mbp expression between control and Runx2 KO mice. (C) Quantification of Mpz and Mbp protein levels, normalized to glyceraldehyde-3-phosphate dehydrogenase (GAPDH) from three independent western blots. (D) Body weight of male control and Runx2 KO mice at 21, 30, and 60 days of age, $n = 8$, Student's t-test. (E) Body weight of female control ($Runx2^{fl/fl}$ CRE-negative mice) and Runx2 KO mice at 21, 30, and 60 days of age $n = 8$, Student's t-test. (F) Normalized Runx2 mRNA count (Reads Per Kilobase per Million mapped reads: RPKM) in the sciatic nerve of wild-type mice from embryonic day 13 and day 17 (E13, E17), postnatal (P) days 1, 5, 14, 24, and 60, and 5 days post-injury (5DI) in adult mice; data from GSE137870 and GSE108231. Data are presented as the mean ± SEM. (G–J) Runx2 is up-regulated in Schwann cells associated with the tibial nerve on day 7 following sciatic nerve transection in control green fluorescent protein (GFP) mice ($Runx2^{fl/fl}$:Cre^{-}). (K–N) Runx2 is undetectable in Schwann cells associated with the tibial nerve on day 7 following sciatic nerve transection in Runx2 KO GFP mice ($Runx2^{fl/fl}$:Cre^{+}). Blue in G and K indicates cell nuclei, green in H and L indicates GFP-positive Schwann cells, and red in I and M indicates Runx2. Scale bars: 50 μm. Ho: Hoechst.

semi-thin sections of tibial nerve (**Figure 4A** and **B**) and transmission electron microscopy images of tibial nerve sections (**Figure 4C** and **D**) showed normal myelination, unaltered axon diameter, and unchanged G-ratios in 2-month-old Runx2 KO mice compared with controls (**Figure 4E–G**).

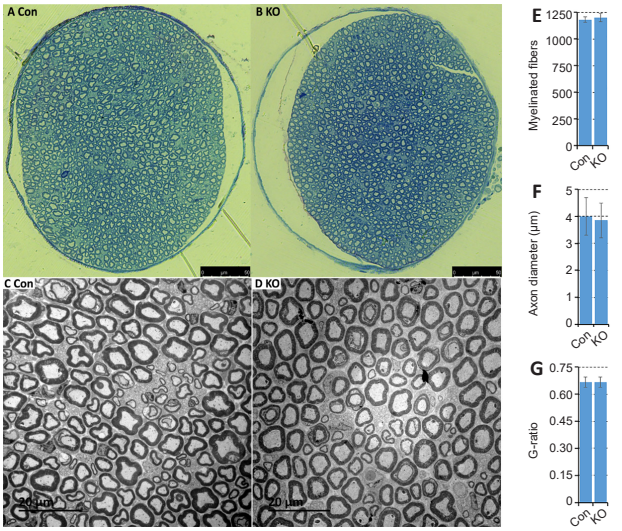

Figure 4 | **Normal peripheral nerve development in Schwann cell-specific Runx2 knockout mice.**
(A, B) Toluidine blue staining of tibial nerve semi-thin sections from 2-month-old control (Con; A) and Runx2 knockout (KO) mice (B). (C, D) Transmission electron microscope images of tibial nerves from 2-month-old control (C) and Runx2 KO mice (D). Scale bars: 50 μm in A and B, 20 μm in C and D. (E) Quantifying the number of myelinated fibers in the tibial nerves of 2-month-old control and Runx2 KO mice, $n = 3$. (F) Axon diameter of myelinated fibers in 2-month-old control and Runx2 KO mice, $n = 3$. (G) G-ratio of tibial nerves from 2-month-old control and Runx2 KO mice, $n = 3$. Data are presented as the mean ± SEM.

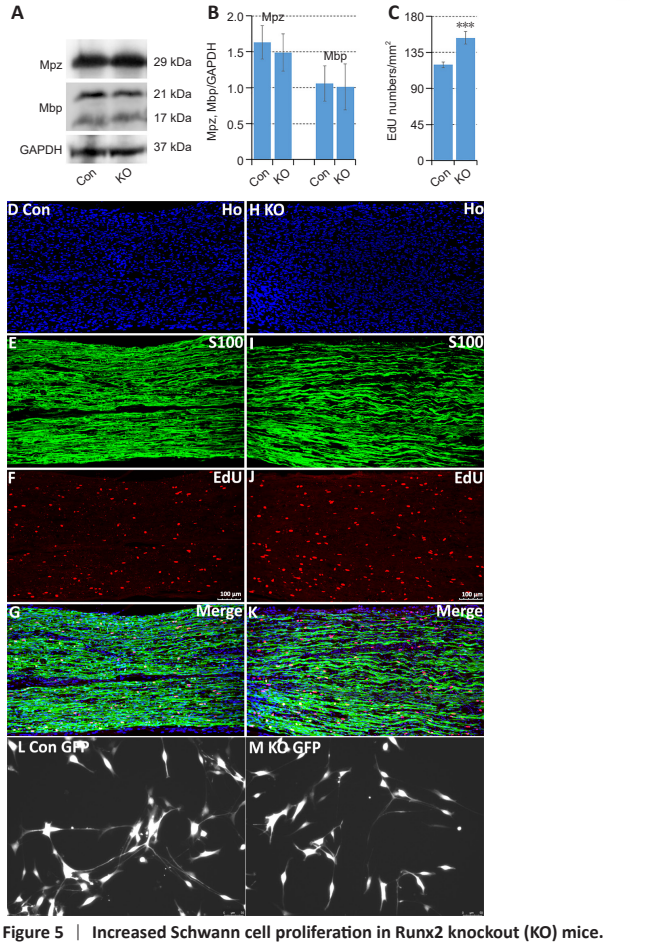

Figure 5 | **Increased Schwann cell proliferation in Runx2 knockout (KO) mice.**
(A) Western blot comparing myelin protein zero (Mpz) and myelin basic protein (Mbp) expression levels in the distal sciatic nerve between control and Runx2 KO mice on day 7 post-injury. (B) Quantification of Mpz and Mbp protein levels, normalized to glyceraldehyde-3-phosphate dehydrogenase (GAPDH), from three independent western blots on day 7 post-injury. (C) Quantification of 5-ethynyl-2′-deoxyuridine (EdU)-positive Schwann cells in the distal sciatic nerve of control and Runx2 KO mice on day 7 post-injury, $n = 4$. (D-G) EdU and S100 staining of the distal sciatic nerve of control mice on day 7 post-injury. (H–K) EdU and S100 staining of the distal sciatic nerve of Runx2 KO mice on day 7 post-injury. Blue in D and H indicates cell nuclei, green in E and I indicates S100 staining in Schwann cells, and red in F and J indicates EdU staining in cell nuclei. (L–M) Morphology of cultured Schwann cells from control green fluorescent protein (GFP; L) and Runx2 KO GFP mice (M). GFP is shown in white. ***$P < 0.001$, *vs*. control group. The scale bar in D (100 μm) applies to D–K. Scale bars in L and M are 100 μm.

Increased Schwann cell proliferation in Runx2 KO nerves following injury

Hung et al. (2015) showed that Runx2 up-regulation in Schwann cells is controlled by c-Jun, a transcription factor that reprograms Schwann cells into a repair-competent cell type following injury (Parkinson et al., 2008; Arthur-Farraj et al., 2012). Thus, we next analyzed Schwann cell de-differentiation and proliferation in Runx2 KO mice (Parkinson et al., 2004; Arthur-Farraj et al., 2012; Gomez-Sanchez et al., 2015; Huang et al., 2015). At 7 days following sciatic nerve transection injury, we harvested the tibial nerves and examined Mpz and Mbp clearance by western blot. In contrast to the impaired myelin clearance seen in c-Jun knockout mice (Fontana et al., 2012), myelin clearance was normal in Runx2 KO mice on day 7 post-injury (**Figure 5A** and **B**). Next, we studied Schwann cell proliferation *in vivo* at day 7 post-injury by EdU injection. EdU/S100 double staining of longitudinal cryosections of the distal sciatic nerve (**Figure 5D–K**) showed that there were significantly more EdU-positive Schwann cells in the distal sciatic nerve of Runx2 KO mice than in control mice ($P < 0.001$; **Figure 5C**), which suggests that Runx2 inhibits Schwann cell proliferation following nerve crush injury.

A previous study showed that loss of c-Jun results in Schwann cell morphological changes *in vitro*: the cells lose their typical bipolar shape and become round and flat (Arthur-Farraj et al., 2012). When we analyzed cultured Schwann cells from adult control GFP and Runx2 KO GFP mice, we found that the Runx2 null Schwann cells still exhibited a typical bipolar shape (**Figure 5L** and **M**). The different effects of Runx2 and c-Jun on myelin clearance, cell proliferation, and morphology demonstrate that, although Runx2 is a c-Jun target (**Figure 2K**), these two proteins have distinct roles in Schwann cell function following injury.

Runx2 promotes Schwann cell migration into the nerve bridge following injury

Following a nerve transection injury, Schwann cells from both the proximal and distal nerve stumps migrate into the gap, alongside nerve fibroblasts, endothelial cells, and immune cells, to form new tissue, known as the nerve bridge (Parrinello et al., 2010; Cattin et al., 2015; Chen et al., 2019; Min et al., 2020). Here, we used two approaches to study control and Runx2 KO Schwann cell migration. First, using mice with the PLP-GFP transgene, we measured Schwann cell migration following injury in control and Runx2 KO nerves *in vivo*. At 6 days post-transection injury, nerve and nerve bridge tissue were harvested, and samples were cleared for imaging using glycerol treatment to assess migration of GFP-positive Schwann cells into the nerve bridge (Dun and Parkinson, 2015, 2018; Chen et al., 2019; Dun et al., 2019). In control mice, large numbers of GFP-positive Schwann cells from both the proximal and distal nerve ends migrated into the bridge (**Figure 6A**). In some nerves from control mice, migrating Schwann cells from both nerve ends had even met in the middle of the nerve bridge at this timepoint (**Figure 6B**). In contrast, fewer migrating Schwann cells were observed in Runx2 KO mice at day 6 (**Figure 6C**). Measuring the total area of migrating Schwann cells in the nerve bridge revealed that Schwann cell migration into the nerve bridge was significantly impaired in Runx2 KO mice compared with control mice (**Figure 6D**). Second, we used a nerve explant culture approach that has been previously used to measure Schwann cell migration (Wang et al., 2012; Shin et al., 2017). We cultured tibial nerve explants (2 mm in length) from both control PLP-GFP mice and Runx2 KO PLP-GFP mice and examined *in vitro* Schwann cell migration. Live-cell images were taken after 150 hours of culturing (**Figure 6F** and **G**), and the number of GFP-positive Schwann cells migrating from each explant was counted. In line with the *in vivo* Schwann cell migration data, significantly fewer migrating Schwann cells were observed in Runx2 KO nerve explants comparing with control nerve explants (**Figure 6E**). Thus, both *in vivo* and *in vitro* approaches showed that Runx2 promotes Schwann cell migration following nerve injury.

Schwann cell-specific Runx2 knockout inhibits axon regeneration and transiently delays functional recovery following crush injury

Following injury, Schwann cells play a major role in producing neurotrophins and providing a substrate for axonal regrowth. This regeneration process is best visualized by whole-mount staining using a neurofilament heavy chain antibody to identify regrowing axons (Dun and Parkinson, 2015, 2018a, b). At 7 days post-crush injury, we observed a clear and significant reduction in the axonal growth rate from the crush site in Runx2 KO animals compared with control animals ($P < 0.001$; **Figure 7A**). Next, we assessed functional recovery by SSI measurement. Before injury, as well at 7 day post-injury, there was no difference in SSI score between the control and Runx2 KO mice. However, Runx2 KO mice exhibited significantly lower SSI scores than control animals on days 11 and 13 post-injury ($P < 0.05$). This delay was transient, as there was no significant difference in SSI between control and Runx2 KO mice from day 15 onwards (**Figure 7B**). Thus, loss of Runx2 expression in Schwann cells inhibited axon regeneration and transiently delayed functional recovery following nerve crush injury.

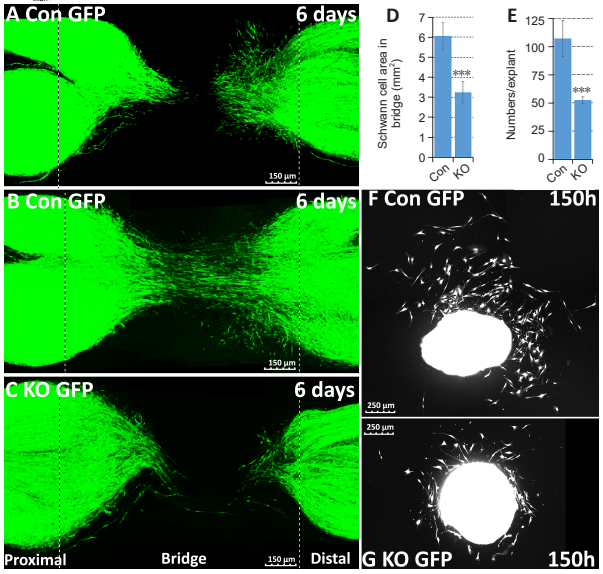

Figure 6 | **Runx2 promotes Schwann cell migration.**
(A) Migrating Schwann cells in the sciatic nerve bridge of control green fluorescent protein (GFP) mice on 6 days following sciatic nerve transection injury; a short distance between migrating Schwann cells from both nerve ends is still visible. (B) Migrating Schwann cells in the sciatic nerve bridge of control GFP mice; Schwann cells from both nerve ends made contact in the nerve bridge on day 6 following sciatic nerve transection injury. (C) Migrating Schwann cells in the sciatic nerve bridge of Runx2 knockout (KO) GFP mice on day 6 following sciatic nerve transection injury. (D) Quantification the total area of migrating Schwann cells in the sciatic nerve bridge of control GFP and Runx2 KO GFP mice on day 6 after sciatic nerve transection injury, $n = 4$. (E) Quantification of migrating Schwann cells in tibial nerve explants from control GFP and Runx2 KO GFP mice, n=4. (F) Migrating Schwann cells from tibial nerve explants from control GFP mice at 150 hours of culture. (G) Migrating Schwann cells from tibial nerve explants from Runx2 KO GFP mice at 150 hours of culture. GFP is shown in white. Data are presented as the mean ± SEM. ***$P < 0.001$, *vs.* control group (Student's *t*-test). Scale bars: 150 μm in A–C, 250 μm in F and G.

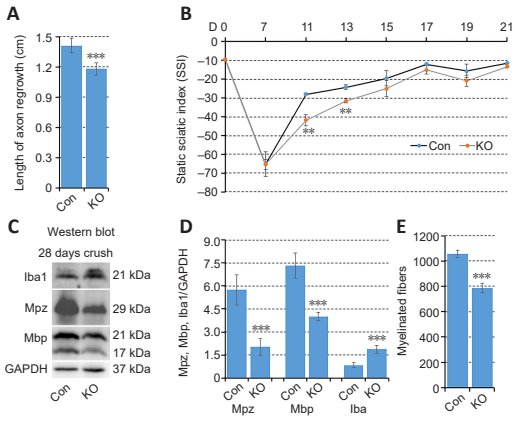

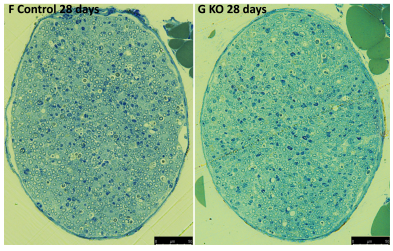

Figure 7 | **Runx2 promotes axon regeneration and Schwann cell re-myelination.**
(A) The length of leading regenerating axons from the crush site on day 7 post-injury in control and Runx2 knockout (KO) mice, $n = 5$. (B) Static sciatic index (SSI) of control and Runx2 KO mice after sciatic nerve crush injury. Runx2 KO mice show significant delays in functional recovery on days 11 and 13 post-injury, $n = 3$. (C) Western blot comparing the levels of ionized calcium binding adaptor molecule 1 (Iba1), myelin protein zero (Mpz), and myelin basic protein (Mbp) expression in the tibial nerves between control and Runx2 KO mice on day 28 following sciatic nerve crush injury. (D) Quantification of Iba1, Mpz, and Mbp protein levels, normalized to 4′,6-diamidino-2-phenylindole (GAPDH), from three independent western blots on day 28 post-injury. (E) Quantifying the number of myelinated fibers on day 28 post-injury in tibial nerve semi-thin sections from control and Runx2 KO mice following toluidine blue staining, $n = 3$. Data are presented as the mean ± SEM. ***$P < 0.001$, *vs.* control group (Student's *t*-test). (F, G) Toluidine blue staining of tibial nerve semi-thin sections from control (F) and Runx2 KO mice (G) on day 28 post-injury. Scale bars: 50 μm.

Runx2 is required for Schwann cell re-myelination

Although Runx2 is not expressed during nerve development (**Figure 3F**), the regulation of its expression by cAMP (**Figure 2I**) implies that it plays a role in re-myelination following injury. Previously, Ding et al. (2018) showed that cAMP treatment up-regulates Runx2 expression in cultured rat primary Schwann cells. We therefore assessed expression levels of the myelin proteins Mpz and Mbp in the tibial nerve by western blot on day 28 post-crush injury. The results showed that Mpz and Mbp were expressed at significantly lower levels in Runx2 KO mice compared with control mice ($P < 0.001$; **Figure 7C** and **D**). Next, we examined the tibial nerve structure in semi-thin sections (**Figure 7F** and **G**) and found that the number of myelinated axons in Runx2 KO nerves was significantly ($P < 0.001$) reduced compared with nerves from control mice (**Figure 7E**). We further examined tibial nerve re-myelination by TEM (**Figure 8A** and **B**) and noted significant differences in G-ratio and myelin thickness on day 28 post-crush injury between control and Runx2 KO mice (**Figure 8C** and **D**), although the diameter of the myelinated axons was similar between control and Runx2 KO mice (**Figure 8E**). Furthermore, there was a significant ($P < 0.001$) decrease in the number of myelinated axons in Runx2 KO mice compared with control mice (**Figure 8L**). In addition, Mbp and neurofilament heavy chain double immunostaining of tibial nerve cryosections showed reduced myelinated axon density in Runx2 KO mice (**Figure 8F–K**). Quantifying the number of total axons in the tibial nerve on day 28 following sciatic nerve crush injury (**Figure 9A–F**) showed that there was no difference in axon numbers or density between the control and Runx2 KO mice (**Figure 9G** and **H**). Thus, the reduced number of myelinated axons resulted from impaired Schwann cell re-myelination rather than a reduced number of nerve fibers.

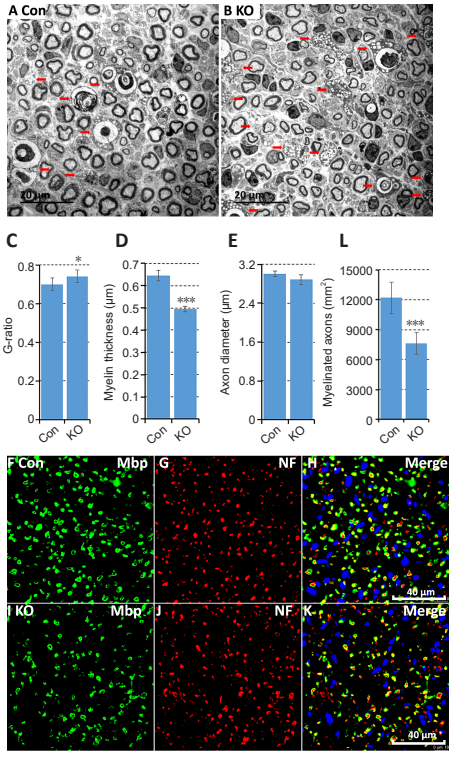

Figure 8 | **Tibial nerve structure of control and Runx2 knockout (KO) mice.**
(A, B) Transmission electron microscope images of tibial nerves from control (Con; A) and Runx2 KO mice (B) on day 28 post-injury. Red arrows indicate macrophages. (C–E, L) G-ratio of remyelinated tibal nerves (C), average myelin thickness (D), average diameter of myelinated axons (E), and myelinated axons per mm^2 (L) in tibial nerves from control and Runx2 KO mice on day 28 post-injury, $n = 3$. *$P < 0.05$, ***$P < 0.001$, *vs.* control group (Student's *t*-test). (F–H) myelin basic protein (Mbp; green) and neurofilament heavy chain (NF; red) double staining of tibial nerve cryosections from control mice on day 28 post-injury. (I–K) Mbp (green) and neurofilament heavy chain (red) double staining of tibial nerve cryosections from Runx2 KO mice on day 28 post-injury. Myelinated axons were quantified by the Mbp staining shown in (F–K). Scale bars: 20 μm in A and B; 40 μm in H and K.

Impaired macrophage clearance in Runx2 KO mice

In addition to reduced re-myelination of axons in Runx2 KO mice, examination of the TEM images clearly showed that there were significantly ($P < 0.05$) more macrophages in the tibial nerves of Runx2 KO mice on day 28 post-crush injury compared with control mice (**Figure 8A** and **B**). Preliminary western blotting of sciatic nerve tissue on 28 days post-injury with the pan-macrophage marker Iba1 showed a significant ($P < 0.001$) increase in Iba1 expression in Runx2 KO mice compared with control mice (**Figure 7C** and **D**). These observations led us to carry out a more detailed exploration of macrophage recruitment and clearance in nerves by immunostaining

tibial nerves for Iba1, a macrophage marker (**Figure 10A–L**). On day 21 post-injury there was no significant difference (P = 0.1191) in macrophage numbers between control and Runx2 KO mice (**Figure 10M**), indicating that macrophage recruitment was not affected in Runx2 KO mice. On day 28 post-injury, the number of macrophages was significantly (P < 0.05) reduced in the tibial nerves of control mice compared with day 21 post-injury (**Figure 10M**), showing rapid macrophage clearance from the tibial nerve in the fourth week of regeneration. However, macrophage clearance was impaired in Runx2 KO mice (**Figure 10M** and **N**).

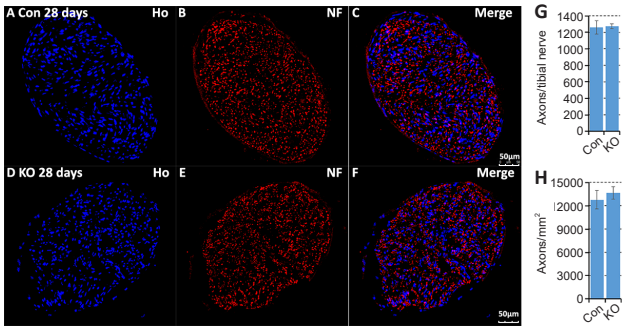

Figure 9 | Normal density of regenerated axons in Runx2 knockout (KO) mice.
(A–F) Neurofilament heavy chain (NF) and Hoechst (Ho) staining of tibial nerve sections from control (Con; A–C) and Runx2 KO (D–F) mice on day 28 after sciatic nerve crush injury. (G, H) Axon numbers per tibial nerve (G) and axon density in tibial nerves (H) from control and Runx2 KO mice on day 28 after sciatic nerve crush injury, n = 3. Blue indicates cell nuclei and red indicates axons. Scale bars: 50 μm.

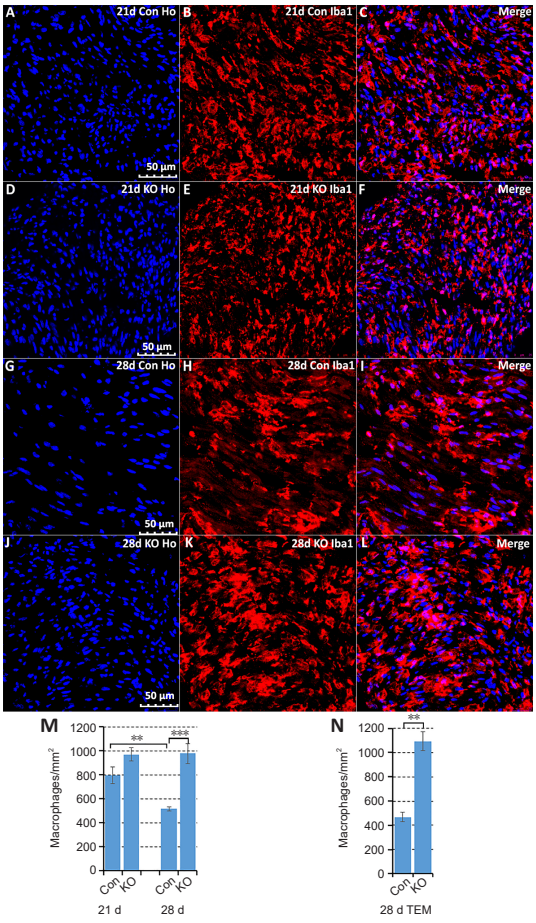

Figure 10 | Impaired macrophage clearance in Runx2 knockout (KO) mice.
(A–F) Iba1 staining of tibial nerve sections from control (A–C) and Runx2 KO mice (D–F) on day 21 after sciatic nerve crush injury. (G–L) Iba1 staining of tibial nerve sections from control (G–I) and Runx2 KO mice (J–L) on day 28 after sciatic nerve crush injury. Blue indicates cell nuclei, and red indicates macrophages. Scale bars: 50 μm. (M) Macrophage density in tibial nerves from control and Runx2 KO mice on days 21 and 28 after sciatic nerve crush injury, as quantified by Iba1 immunostaining, n = 4. (N) Macrophage density in tibial nerves from control and Runx2 KO mice on day 28 after sciatic nerve crush injury, as quantified on transmission electron microscope images, n = 3. Data are presented as the mean ± SEM. **P < 0.01, ***P < 0.001 (Student's t-test).

Discussion

The identification of signaling pathways and transcription factors regulating Schwann cell plasticity is vital to our understanding, not only of what controls peripheral nerve development, but also of what controls peripheral nerve repair after injury (Jessen and Mirsky, 2005, 2008). During development, Schwann cells express negative regulators of myelination, such as c-Jun, Sox2, Pax3, and Id2, to time the onset of peripheral myelination (Jessen and Mirsky, 2008). Peripheral myelination is controlled by the well-known transcription factors Sox10, Oct6, and Krox20 (Jessen and Mirsky, 2008; Parkinson et al., 2008; Woodhoo et al., 2009; Doddrell et al., 2012). These negative transcription factors are re-expressed after peripheral nerve injury to promote Schwann cell dedifferentiation and proliferation, processes that are required to reverse Schwann cells from a mature stage to a regenerative phenotype (Jessen and Mirsky, 2008, 2016). Recent microarray and mRNA sequencing data indicate that there are many more transcription factors involved in this intriguing repair process, but their function in peripheral nerve repair remains unclear (Barrette et al., 2010; Arthur-Farraj et al., 2012; Clements et al., 2017; Pan et al., 2017). One transcription factor that is dramatically up-regulated following peripheral nerve injury is Runx2 (Hung et al., 2015; Arthur-Farraj et al., 2017). To understand the role of Runx2 in Schwann cells during peripheral nerve regeneration, in this study we performed both *in vitro* and *in vivo* experiments and found that the main function of Runx2 is to promote Schwann cell re-myelination.

Runx2 belongs to the family of runt-related transcription factors, three members of which, Runx1, Runx2, and Runx3, have been identified in mammals (Schroeder et al., 2005; Bruderer et al., 2014). Gene knockout studies have revealed well-defined biological roles for the Runx proteins. Runx1 is indispensable for definitive haematopoiesis, as Runx1$^{-/-}$ mice lack fetal liver-derived definitive haematopoiesis (Wang et al., 1996). Runx2$^{-/-}$ mice die just after birth, showing complete absence of bone formation. Analysis of Runx2$^{-/-}$ mice revealed that they failed to achieve osteoblast differentiation, indicating that Runx2 is essential for bone development and homeostasis in mice (Komori et al., 1997; Otto et al., 1997). Runx3$^{-/-}$ mice exhibit loss of proprioceptive neurons in dorsal root ganglia, resulting in the development of severe limb ataxia due to disruption of monosynaptic connectivity between intraspinal afferents and motoneurons (Inoue et al., 2002; Levanon et al., 2002).

The best-known function of Runx2 is as the master regulator of bone development (Bruderer et al., 2014). During skeletal development, Runx2 is weakly expressed in proliferating chondrocytes, and its expression induces Indian hedgehog (Ihh) expression, which is required for chondrocyte proliferation; thus, Runx2 expression in proliferating chondrocytes promotes chondrocyte proliferation through the induction of Ihh expression (Komori, 2020). Runx2 expression is up-regulated in prehypertrophic chondrocytes, and this up-regulation is required for the differentiation (maturation) of prehypertrophic chondrocytes to hypertrophic chondrocytes, as indicated by a lack of hypertrophic chondrocyte layers throughout most of the skeleton in Runx2$^{-/-}$ mice (Komori, 2019, 2020). Runx2 is also expressed in bone mesenchymal stem cells during skeletal development, and its expression is up-regulated in preosteoblasts. Runx2 expression reaches the maximum level in immature osteoblasts, and it is then down-regulated in mature osteoblasts (Inoue et al., 2002; Fry et al., 2007; Komori, 2019, 2020). Runx2 regulates Fgfr2 and Fgfr3 expression in osteoprogenitors, and Fgf signaling promotes osteoprogenitor proliferation (Inoue et al., 2002; Komori, 2019, 2020). However, Runx2 plays an anti-proliferative role in preosteoblasts. *In vitro* studies have shown that Runx2 inhibits the proliferation of osteoblast-lineage cells or mesenchymal stem cells (Pratap et al., 2003; Galindo et al., 2005). An *in vitro* study also demonstrated that Runx2$^{-/-}$ calvarial cells proliferate faster than control calvarial cells (Kawane et al., 2018). Gene expression profile analysis indicated that the expression of cell cycle-related genes in wild-type calvaria tissue is different from that seen in calvaria-derived Runx2$^{-/-}$ cells (Kawane et al., 2018). These findings indicate that Runx2 is required for preosteoblast differentiation but not proliferation. Thus, whether Runx2 promotes cell proliferation or regulates cell differentiation depends on the cell type.

Owing to the perinatal death of Runx2$^{-/-}$ mice, we crossed the Runx2 conditional gene knockout mice (Runx2$^{fl/fl}$) (Ferrari et al., 2015) with Schwann cell-specific Cre mice (MPZ-Cre) (Feltri et al., 1999) to generate Schwann cell-specific Runx2 KO mice and examine the function of Runx2 in peripheral nerve development and repair. We showed that loss of Runx2 expression in Schwann cells had no effect on peripheral nerve development. Schwann cell-specific Runx2 KO mice exhibited normal body weight and peripheral nerve structure. Analyzing mRNA sequencing data also indicated that Runx2 was not expressed in either developing or adult mouse sciatic nerve, suggesting that Runx2 functions as an injury-induced transcription factor in the peripheral nervous system. We found that loss of Runx2 in Schwann cells increased Schwann cell proliferation following sciatic nerve injury, indicating that up-regulation of Runx2 in Schwann cells following peripheral nerve injury inhibits Schwann cell proliferation. Although Tgfβ1 up-regulates Runx2 expression in osteoblasts, we found that Tgfβ1 inhibited Runx2 expression in Schwann cells. Tgfβ1 promotes Schwann cell proliferation rather than differentiation following peripheral nerve injury (Clements et al., 2017), which further supports our finding that Runx2 inhibits Schwann cell proliferation.

We observed that Runx2 and c-Jun have different effects on Schwann cell myelin clearance, proliferation, and morphology, and therefore we compared

Runx2 up-regulation in Schwann cell-specific c-Jun knockout mice with control mice by analyzing previously published microarray data GSE38693 (Arthur-Farraj et al., 2012). Our analysis showed that Runx2 was up-regulated 42.5-fold in the distal nerve following sciatic nerve injury in control mice, while it was only up-regulated 15.6-fold in Schwann cell-specific c-Jun knockout mice; thus, Runx2 up-regulation was significantly reduced in c-Jun knockout mice compared with control mice. However, our results revealed that the major function of Runx2 in Schwann cells differed from that of c-Jun, despite c-Jun regulating Runx2 expression in Schwann cells.

Schwan cell re-myelination is impaired in Runx2 KO mice. We showed that Btc and Fgf5 up-regulated Runx2 expression in cultured primary rat Schwann cells. Previous studies have shown that Btc and Fgf signaling promote peripheral nerve regeneration and Schwann cell re-myelination (Grothe et al., 2006; Haastert et al., 2008; Vallieres et al., 2017). Furthermore, treating cultured primary rat Schwann cells with cAMP up-regulated Runx2 expression. These findings provide additional evidence that Runx2 promotes Schwann cell re-myelination during peripheral nerve regeneration. In addition, the results from the Btc, Tnc, and Fgf5 treatment experiments showed that multiple signaling pathways, though not the TGFβ1 signaling pathway, up-regulate Runx2 expression in Schwann cells. Taken together, our results showed that Runx2 up-regulation in Schwann cells is required for Schwann cell re-differentiation during peripheral nerve regeneration. Following peripheral nerve injury in adult mice, the speed of axon regrowth in Runx2 KO mice was slower than that seen in control mice. Furthermore, functional recovery was transiently delayed in Runx2 KO mice, and loss of Runx2 in Schwann cells inhibited Schwann cell migration.

Both our TEM and Iba1 immunostaining results confirmed that there were significantly more macrophages in tibial nerves of Runx2 KO mice than control mice at day 28 following sciatic nerve crush injury. However, the numbers of macrophages in the tibial nerve were similar between control and Runx2 KO mice at day 21 following sciatic nerve crush injury, indicating that loss of Runx2 in Schwann cells impaired macrophage clearance but had no effect on macrophage recruitment. Previously, Fry et al. (2007) showed that macrophage clearance during peripheral nerve regeneration is controlled by Schwann cell re-myelination. Infiltrated macrophages in injured peripheral nerves exhibited increased expression of the Nogo receptors NgR1 and NgR2 on the cell surface in the first week after injury. Upon onset of Schwann cell re-myelination, myelin produced by Schwann cells binds to Nogo receptors on the surface of macrophages and activates Rho-associated kinase in macrophages to promote macrophage clearance (Fry et al., 2007). Fry et al. (2007) compared macrophage clearance from the distal nerve following rat sciatic nerve crush injury because transection injury prevents axon regeneration and Schwann cell re-myelination. Fourteen days post-crush injury, regenerated nerves with newly synthesized myelin exhibited fewer macrophages than transected nerves that lack axons and myelin. Almost all macrophages in the transected nerves still lay within the Schwann cell basal lamina, while in the crushed and regenerated nerves the majority of the macrophages had migrated out of the Schwann cell basal lamina (Fry et al., 2007). We showed that Schwann cell re-meylination was impaired in Runx2 KO mice, and the number of myelinated fibers in the tibial nerves of Runx2 KO mice was significantly lower than that seen in control mice. Therefore, impaired re-meylination in Schwann cell-specific Runx2 KO mice could prevent macrophages expressing Nogo receptors from being activated, thereby impairing macrophage clearance.

A major limitation of this study is that we did not explore the expression of any Runx2 targets. Studying Runx2 targets could provide a better understanding of the function of Runx2 in peripheral nerve regeneration.

In conclusion, we showed that Runx2 was up-regulated in Schwann cells following peripheral nerve injury, and that multiple factors, such as Fgf5, Tenascin C (Tnc), and betacellulin (Btc), in the injured nerves could regulate Runx2 expression in Schwann cells. Using Schwann cell-specific Runx2 knockout mice, we found that loss of Runx2 had no discernible effect on peripheral nerve development but had multiple consequences during peripheral nerve repair, including impaired Schwann cell proliferation, Schwann cell migration, nerve re-myelination, axonal regrowth, and macrophage clearance. Taken together, our findings indicate that Runx2 plays a major role in Schwann cell migration, re-myelination, and peripheral nerve functional recovery following injury. Thus, manipulating signaling pathways that promote Runx2 expression in Schwann cells could benefit successful peripheral repair following injury.

Acknowledgments: *We would like to thank Professor Karen Blyth (School of Cancer Sciences, University of Glasgow, UK) for providing us Runx2$^{flox/flox}$ mouse breeding pairs. We also thank Professor David B. Parkinson (Faculty of Health, University of Plymouth, Plymouth, UK) for critically reading the manuscript.*
Author contributions: *RH and LS performed the experiments and data analysis. MCB analyzed the scRNA-seq data. XD designed the study and wrote the paper. All authors approved the final version of the manuscript.*
Conflicts of interest: *The authors declare that there is no conflict of interests existing for this study.*
Data availability statement: *No additional data are available.*

References

Allodi I, Mecollari V, Gonzalez-Perez F, Eggers R, Hoyng S, Verhaagen J, Navarro X, Udina E (2014) Schwann cells transduced with a lentiviral vector encoding Fgf-2 promote motor neuron regeneration following sciatic nerve injury. Glia 62:1736-1746.

Arthur-Farraj PJ, Latouche M, Wilton DK, Quintes S, Chabrol E, Banerjee A, Woodhoo A, Jenkins B, Rahman M, Turmaine M, Wicher GK, Mitter R, Greensmith L, Behrens A, Raivich G, Mirsky R, Jessen KR (2012) c-Jun reprograms Schwann cells of injured nerves to generate a repair cell essential for regeneration. Neuron 75:633-647.

Arthur-Farraj PJ, Morgan CC, Adamowicz M, Gomez-Sanchez JA, Fazal SV, Beucher A, Razzaghi B, Mirsky R, Jessen KR, Aitman TJ (2017) Changes in the coding and non-coding transcriptome and DNA methylome that define the Schwann cell repair phenotype after nerve injury. Cell Rep 20:2719-2734.

Baptista AF, Gomes JR, Oliveira JT, Santos SM, Vannier-Santos MA, Martinez AM (2007) A new approach to assess function after sciatic nerve lesion in the mouse- adaptation of the sciatic static index. J Neurosci Methods 161:259-264.

Barrette B, Calvo E, Vallieres N, Lacroix S (2010) Transcriptional profiling of the injured sciatic nerve of mice carrying the Wld(S) mutant gene: identification of genes involved in neuroprotection, neuroinflammation, and nerve regeneration. Brain Behav Immun 24:1254-1267.

Bruderer M, Richards RG, Alini M, Stoddart MJ (2014) Role and regulation of RUNX2 in osteogenesis. Eur Cell Mater 28:269-286.

Carr MJ, Toma JS, Johnston APW, Steadman PE, Yuzwa SA, Mahmud N, Frankland PW, Kaplan DR, Miller FD (2019) Mesenchymal precursor cells in adult nerves contribute to mammalian tissue repair and regeneration. Cell Stem Cell 24:240-256 e249.

Cattin AL, Burden JJ, Van Emmenis L, Mackenzie FE, Hoving JJ, Garcia Calavia N, Guo Y, McLaughlin M, Rosenberg LH, Quereda V, Jamecna D, Napoli I, Parrinello S, Enver T, Ruhrberg C, Lloyd AC (2015) Macrophage-induced blood vessels guide schwann cell-mediated regeneration of peripheral nerves. Cell 162:1127-1139.

Chen B, Chen Q, Parkinson DB, Dun XP (2019) Analysis of Schwann cell migration and axon regeneration following nerve injury in the sciatic nerve bridge. Front Mol Neurosci 12:308.

Chen B, Hu R, Min Q, Li Y, Parkinson DB, Dun XP (2020) FGF5 regulates Schwann cell migration and adhesion. Front Cell Neurosci 14:237.

Chen B, Banton MC, Singh L, Parkinson DB, Dun XP (2021) Single cell transcriptome data analysis defines the heterogeneity of peripheral nerve cells in homeostasis and regeneration. Front Cell Neurosci 15:624826.

Cintron-Colon AF, Almeida-Alves G, VanGyseghem JM, Spitsbergen JM (2022) GDNF to the rescue: GDNF delivery effects on motor neurons and nerves, and muscle re-innervation after peripheral nerve injuries. Neural Regen Res 17:748-753.

Clements MP, Byrne E, Camarillo Guerrero LF, Cattin AL, Zakka L, Ashraf A, Burden JJ, Khadayate S, Lloyd AC, Marguerat S, Parrinello S (2017) The wound microenvironment reprograms schwann cells to invasive mesenchymal-like cells to drive peripheral nerve regeneration. Neuron 96:98-114. e117.

Cohen MM Jr (2009) Perspectives on RUNX genes: an update. Am J Med Genet A 149A:2629-2646.

Ding D, Zhang P, Liu Y, Wang Y, Sun W, Yu Z, Cheng Z, Wang Y (2018) Runx2 was correlated with neurite outgrowth and Schwann cell differentiation, migration after sciatic nerve crush. Neurochem Res 43:2423-2434.

Doddrell RD, Dun XP, Moate RM, Jessen KR, Mirsky R, Parkinson DB (2012) Regulation of Schwann cell differentiation and proliferation by the Pax-3 transcription factor. Glia 60:1269-1278.

Doddrell RD, Dun XP, Shivane A, Feltri ML, Wrabetz L, Wegner M, Sock E, Hanemann CO, Parkinson DB (2013) Loss of SOX10 function contributes to the phenotype of human Merlin-null schwannoma cells. Brain 136:549-563.

Dun XP, Parkinson DB (2015) Visualizing peripheral nerve regeneration by whole mount staining. PLoS One 10:e0119168.

Dun XP, Parkinson DB (2018a) Transection and crush models of nerve injury to measure repair and remyelination in peripheral nerve. Methods Mol Biol 1791:251-262.

Dun XP, Parkinson DB (2018b) Whole mount immunostaining on mouse sciatic nerves to visualize events of peripheral nerve regeneration. Methods Mol Biol 1739:339-348.

Dun XP, Carr L, Woodley PK, Barry RW, Drake LK, Mindos T, Roberts SL, Lloyd AC, Parkinson DB (2019) Macrophage-derived Slit3 controls cell migration and axon pathfinding in the peripheral nerve bridge. Cell Rep 26:1458-1472 e1454.

Feltri ML, D'Antonio M, Previtali S, Fasolini M, Messing A, Wrabetz L (1999) P0-Cre transgenic mice for inactivation of adhesion molecules in Schwann cells. Ann N Y Acad Sci 883:116-123.

Ferrari N, Riggio AI, Mason S, McDonald L, King A, Higgins T, Rosewell I, Neil JC, Smalley MJ, Sansom OJ, Morris J, Cameron ER, Blyth K (2015) Runx2 contributes to the regenerative potential of the mammary epithelium. Sci Rep 5:15658.

Fontana X, Hristova M, Da Costa C, Patodia S, Thei L, Makwana M, Spencer-Dene B, Latouche M, Mirsky R, Jessen KR, Klein R, Raivich G, Behrens A (2012) c-Jun in Schwann cells promotes axonal regeneration and motoneuron survival via paracrine signaling. J Cell Biol 198:127-141.

Fry EJ, Ho C, David S (2007) A role for Nogo receptor in macrophage clearance from injured peripheral nerve. Neuron 53:649-662.

Galindo M, Pratap J, Young DW, Hovhannisyan H, Im HJ, Choi JY, Lian JB, Stein JL, Stein GS, van Wijnen AJ (2005) The bone-specific expression of Runx2 oscillates during the cell cycle to support a G1-related antiproliferative function in osteoblasts. J Biol Chem 280:20274-20285.

Gomez-Sanchez JA, Carty L, Iruarrizaga-Lejarreta M, Palomo-Irigoyen M, Varela-Rey M, Griffith M, Hantke J, Macias-Camara N, Azkargorta M, Aurrekoetxea I, De Juan VG, Jefferies HB, Aspichueta P, Elortza F, Aransay AM, Martínez-Chantar ML, Baas F, Mato JM, Mirsky R, Woodhoo A, et al. (2015) Schwann cell autophagy, myelinophagy, initiates myelin clearance from injured nerves. J Cell Biol 210:153-168.

Grothe C, Haastert K, Jungnickel J (2006) Physiological function and putative therapeutic impact of the FGF-2 system in peripheral nerve regeneration--lessons from in vivo studies in mice and rats. Brain Res Rev 51:293-299.

Haastert K, Ying Z, Grothe C, Gomez-Pinilla F (2008) The effects of FGF-2 gene therapy combined with voluntary exercise on axonal regeneration across peripheral nerve gaps. Neurosci Lett 443:179-183.

Huang L, Quan X, Liu Z, Ma T, Wu Y, Ge J, Zhu S, Yang Y, Liu L, Sun Z, Huang J, Luo Z (2015) c-Jun gene-modified Schwann cells: upregulating multiple neurotrophic factors and promoting neurite outgrowth. Tissue Eng Part A 21:1409-1421.

Hung HA, Sun G, Keles S, Svaren J (2015) Dynamic regulation of Schwann cell enhancers after peripheral nerve injury. J Biol Chem 290:6937-6950.

Inoue K, Ozaki S, Shiga T, Ito K, Masuda T, Okado N, Iseda T, Kawaguchi S, Ogawa M, Bae SC, Yamashita N, Itohara S, Kudo N, Ito Y (2002) Runx3 controls the axonal projection of proprioceptive dorsal root ganglion neurons. Nat Neurosci 5:946-954.

Jessen KR, Mirsky R (2005) The origin and development of glial cells in peripheral nerves. Nat Rev Neurosci 6:671-682.

Jessen KR, Mirsky R (2008) Negative regulation of myelination: relevance for development, injury, and demyelinating disease. Glia 56:1552-1565.

Jessen KR, Mirsky R (2016) The repair Schwann cell and its function in regenerating nerves. J Physiol 594:3521-3531.

Kawane T, Qin X, Jiang Q, Miyazaki T, Komori H, Yoshida CA, Matsuura-Kawata V, Sakane C, Matsuo Y, Nagai K, Maeno T, Date Y, Nishimura R, Komori T (2018) Runx2 is required for the proliferation of osteoblast progenitors and induces proliferation by regulating Fgfr2 and Fgfr3. Sci Rep 8:13551.

Kiefer R, Streit WJ, Toyka KV, Kreutzberg GW, Hartung HP (1995) Transforming growth factor-beta 1: a lesion-associated cytokine of the nervous system. Int J Dev Neurosci 13:331-339.

Ko KR, Lee J, Nho B, Kim S (2018) c-Fos is necessary for HGF-mediated gene regulation and cell migration in Schwann cells. Biochem Biophys Res Commun 503:2855-2860.

Komori T, Yagi H, Nomura S, Yamaguchi A, Sasaki K, Deguchi K, Shimizu Y, Bronson RT, Gao YH, Inada M, Sato M, Okamoto R, Kitamura Y, Yoshiki S, Kishimoto T (1997) Targeted disruption of Cbfa1 results in a complete lack of bone formation owing to maturational arrest of osteoblasts. Cell 89:755-764.

Komori T (2019) Regulation of proliferation, differentiation and functions of osteoblasts by Runx2. Int J Mol Sci 20:1694.

Komori T (2020) Molecular mechanism of Runx2-dependent bone development. Mol Cells 43:168-175.

Lee KS, Kim HJ, Li QL, Chi XZ, Ueta C, Komori T, Wozney JM, Kim EG, Choi JY, Ryoo HM, Bae SC (2000) Runx2 is a common target of transforming growth factor beta1 and bone morphogenetic protein 2, and cooperation between Runx2 and Smad5 induces osteoblast-specific gene expression in the pluripotent mesenchymal precursor cell line C2C12. Mol Cell Biol 20:8783-8792.

Levanon D, Bettoun D, Harris-Cerruti C, Woolf E, Negreanu V, Eilam R, Bernstein Y, Goldenberg D, Xiao C, Fliegauf M, Kremer E, Otto F, Brenner O, Lev-Tov A, Groner Y (2002) The Runx3 transcription factor regulates development and survival of TrkC dorsal root ganglia neurons. EMBO J 21:3454-3463.

Liu YT, Xu Z, Liu W, Ren S, Xiong HW, Jiang T, Chen J, Kang Y, Li QY, Wu ZH, Machens HG, Yang XF, Chen ZB (2023) The circ_0002538/miR-138-5p/plasmolipin axis regulates Schwann cell migration and myelination in diabetic peripheral neuropathy. Neural Regen Res 18:1591-1600.

Livak KJ, Schmittgen TD (2001) Analysis of relative gene expression data using real-time quantitative PCR and the 2(-Delta Delta C(T)) Method. Methods 25:402-408.

Ma KH, Hung HA, Svaren J (2016) Epigenomic regulation of schwann cell reprogramming in peripheral nerve injury. J Neurosci 36:9135-9147.

Mallon BS, Shick HE, Kidd GJ, Macklin WB (2002) Proteolipid promoter activity distinguishes two populations of NG2-positive cells throughout neonatal cortical development. J Neurosci 22:876-885.

Min Q, Parkinson DB, Dun XP (2020) Migrating Schwann cells direct axon regeneration within the peripheral nerve bridge. Glia 69:235-254.

Mindos T, Dun XP, North K, Doddrell RD, Schulz A, Edwards P, Russell J, Gray B, Roberts SL, Shivane A, Mortimer G, Pirie M, Zhang N, Pan D, Morrison H, Parkinson DB (2017) Merlin controls the repair capacity of Schwann cells after injury by regulating Hippo/YAP activity. J Cell Biol 216:495-510.

Otalora-Otalora BA, Henriquez B, Lopez-Kleine L, Rojas A (2019) RUNX family: Oncogenes or tumor suppressors (Review). Oncol Rep 42:3-19.

Otto F, Thornell AP, Crompton T, Denzel A, Gilmour KC, Rosewell IR, Stamp GW, Beddington RS, Mundlos S, Olsen BR, Selby PB, Owen MJ (1997) Cbfa1, a candidate gene for cleidocranial dysplasia syndrome, is essential for osteoblast differentiation and bone development. Cell 89:765-771.

Pan B, Liu Y, Yan JY, Wang Y, Yao X, Zhou HX, Lu L, Kong XH, Feng SQ (2017) Gene expression analysis at multiple time-points identifies key genes for nerve regeneration. Muscle Nerve 55:373-383.

Parkinson DB, Dong Z, Bunting H, Whitfield J, Meier C, Marie H, Mirsky R, Jessen KR (2001) Transforming growth factor beta (TGFbeta) mediates Schwann cell death in vitro and in vivo: examination of c-Jun activation, interactions with survival signals, and the relationship of TGFbeta-mediated death to Schwann cell differentiation. J Neurosci 21:8572-8585.

Parkinson DB, Bhaskaran A, Droggiti A, Dickinson S, D'Antonio M, Mirsky R, Jessen KR (2004) Krox-20 inhibits Jun-NH2-terminal kinase/c-Jun to control Schwann cell proliferation and death. J Cell Biol 164:385-394.

Parkinson DB, Bhaskaran A, Arthur-Farraj P, Noon LA, Woodhoo A, Lloyd AC, Feltri ML, Wrabetz L, Behrens A, Mirsky R, Jessen KR (2008) c-Jun is a negative regulator of myelination. J Cell Biol 181:625-637.

Parrinello S, Napoli I, Ribeiro S, Wingfield Digby P, Fedorova M, Parkinson DB, Doddrell RD, Nakayama M, Adams RH, Lloyd AC (2010) EphB signaling directs peripheral nerve regeneration through Sox2-dependent Schwann cell sorting. Cell 143:145-155.

Percie du Sert N, Hurst V, Ahluwalia A, Alam S, Avey MT, Baker M, Browne WJ, Clark A, Cuthill IC, Dirnagl U, Emerson M, Garner P, Holgate ST, Howells DW, Karp NA, Lazic SE, Lidster K, MacCallum CJ, Macleod M, Pearl EJ, et al. (2020) The ARRIVE guidelines 2.0: Updated guidelines for reporting animal research. PLoS Biol 18:e3000410.

Pratap J, Galindo M, Zaidi SK, Vradii D, Bhat BM, Robinson JA, Choi JY, Komori T, Stein JL, Lian JB, Stein GS, van Wijnen AJ (2003) Cell growth regulatory role of Runx2 during proliferative expansion of preosteoblasts. Cancer Res 63:5357-5362.

Qin HJ, Li H, Chen JZ, Zhang KR, Zhao XQ, Qin JQ, Yu B, Yang J (2023) Artificial nerve graft constructed by coculture of activated Schwann cells and human hair keratin for repair of peripheral nerve defects. Neural Regen Res 18:1118-1123.

Roberts SL, Dun XP, Doddrell RDS, Mindos T, Drake LK, Onaitis MW, Florio F, Quattrini A, Lloyd AC, D'Antonio M, Parkinson DB (2017) Sox2 expression in Schwann cells inhibits myelination in vivo and induces influx of macrophages to the nerve. Development 144:3114-3125.

Rufer M, Flanders K, Unsicker K (1994) Presence and regulation of transforming growth factor beta mRNA and protein in the normal and lesioned rat sciatic nerve. J Neuroscie Res 39:412-423.

Scherer SS, Kamholz J, Jakowlew SB (1993) Axons modulate the expression of transforming growth factor-betas in Schwann cells. Glia 8:265-276.

Schneider CA, Rasband WS, Eliceiri KW (2012) NIH Image to ImageJ: 25 years of image analysis. Nat Methods 9:671-675.

Schroeder TM, Jensen ED, Westendorf JJ (2005) Runx2: a master organizer of gene transcription in developing and maturing osteoblasts. Birth Defects Res C Embryo Today 75:213-225.

Shin YK, Jang SY, Yun SH, Choi YY, Yoon BA, Jo YR, Park SY, Pak MG, Park JI, Park HT (2017) Cooperative interaction of hepatocyte growth factor and neuregulin regulates Schwann cell migration and proliferation through Grb2-associated binder-2 in peripheral nerve repair. Glia 65:1794-1808.

Toma JS, Karamboulas K, Carr MJ, Kolaj A, Yuzwa SA, Mahmud N, Storer MA, Kaplan DR, Miller FD (2020) Peripheral nerve single-cell analysis identifies mesenchymal ligands that promote axonal growth. eNeuro 7:ENEURO.0066-20.2020.

Vallieres N, Barrette B, Wang LX, Belanger E, Thiry L, Schneider MR, Filali M, Cote D, Bretzner F, Lacroix S (2017) Betacellulin regulates schwann cell proliferation and myelin formation in the injured mouse peripheral nerve. Glia 65:657-669.

Wang Q, Stacy T, Binder M, Marin-Padilla M, Sharpe AH, Speck NA (1996) Disruption of the Cbfa2 gene causes necrosis and hemorrhaging in the central nervous system and blocks definitive hematopoiesis. Proc Natl Acad Sci U S A 93:3444-3449.

Wang Y, Teng HL, Huang ZH (2012) Intrinsic migratory properties of cultured Schwann cells based on single-cell migration assay. PLoS One 7:e51824.

Woodhoo A, Alonso MB, Droggiti A, Turmaine M, D'Antonio M, Parkinson DB, Wilton DK, Al-Shawi R, Simons P, Shen J, Guillemot F, Radtke F, Meijer D, Feltri ML, Wrabetz L, Mirsky R, Jessen KR (2009) Notch controls embryonic Schwann cell differentiation, postnatal myelination and adult plasticity. Nat Neurosci 12:839-847.

Woodley PK, Min Q, Li Y, Mulvey NF, Parkinson DB, Dun XP (2019) Distinct VIP and PACAP functions in the distal nerve stump during peripheral nerve regeneration. Front Neurosci 13:1326.

Zhang Z, Yu B, Gu Y, Zhou S, Qian T, Wang Y, Ding G, Ding F, Gu X (2016) Fibroblast-derived tenascin-C promotes Schwann cell migration through beta1-integrin dependent pathway during peripheral nerve regeneration. Glia 64:374-385.

C-Editors: Zhao LJ, Zhao M; S-Editor: Li CH; L-Editors: Li CH, Song LP; T-Editor: Jia Y